Centennial-scale dynamics of the Southern Hemisphere westerly winds across the Drake Passage over the past two millennia

Zhengyu Xia[1], Zicheng Yu[1,2] and Julie Loisel[3]

[1]*Department of Earth and Environmental Sciences, Lehigh University, Bethlehem, Pennsylvania 18015, USA*

[2]*School of Geographical Sciences, Northeast Normal University, Changchun 130024, China*

[3]*Department of Geography, Texas A&M University, College Station, Texas 77843, USA*

This supplementary file includes

1. Site information
2. Age-depth model and loss-on-ignition results from core PAT16-AP1
3. Macrofossil analysis results from core PAT16-AP1
4. Evaluation of evaporative effect on oxygen isotopes of moss cellulose
5. Air-parcel backward trajectory analysis using HYSPLIT model
6. A close-up look of PAT16-AP1 proxy record for the last 150 years

1. Site information

Ariel Peatland (AP; unofficial name) is an ombrotrophic bog situated in the Karukinka Park, Isla Grande of Tierra del Fuego, Chile (54.20732° S, 68.71739° W; elevation 169 m above sea level). The peatland has a surface area of ~0.5 km^2 and a bog water pH of 4.3 (measured in January 2016). The site is surrounded by forested upland area on the north, south and west, while on the east it opens to a large floodplain, where a meandering river ~250 m away is flowing northward (Fig. DR1). At present the bog surface is relatively dry, in agreement with the fact that it is located at the driest end of the climate space of peat bog ecosystems in southernmost Patagonia (Loisel and Yu, 2013). It is also flat with limited developments of hummock-hollow and pool patterns (Fig. DR1). Single-species *Sphagnum magellanicum* dominates the center of bog, while vascular plants (mixture of herbaceous and ligneous plants) are more abundant near the edge of bog. The vegetation of peat bogs in Patagonia has been described and summarized by Loisel and Yu (2013).

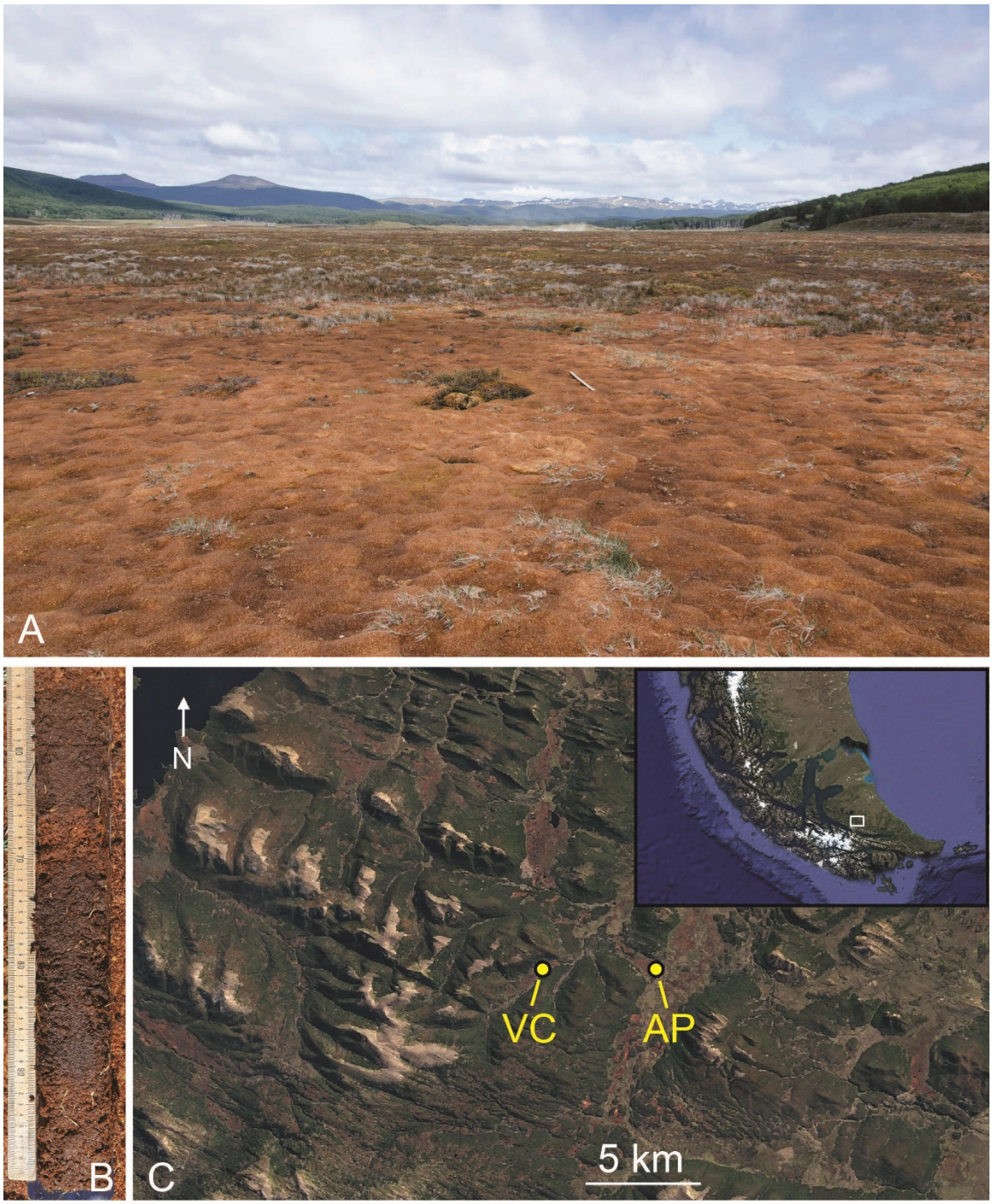

Figure DR1. (A) Field photo of Ariel Peatland (AP) taken from the bog center towards its edge, looking toward east. (B) Core photo of 50–100 cm section from core PAT16-AP1 collected using a Russian peat sampler. (C) Google Earth images showing the geographical context and location of Ariel Peatland and Valle de Consejo (VC), another peatland site discussed below in Section 4. The main image is the "zoom-in" of white square area in inset image on top right.

2. Age-depth model and loss-on-ignition results from core PAT16-AP1

Table DR1. Radiocarbon dates of core PAT16-AP1 from Ariel Peatland.

Lab ID (UCIAMS)	Depth (cm)	Corrected depth (cm)*	Dated material	Radiocarbon age (^{14}C yr BP) or fraction modern (%FM)	δ^{13}C (‰, VPDB)	Median age (cal. yr BP)#	2σ range (cal. yr BP)#
185565	15–16	15.5	*Sphagnum* stems/leaves	113.11 ± 0.17 %FM†	-25.1	-	-
185566	25–26	25.5	*Sphagnum* stems/leaves	131.8 ± 0.2 %FM†	-24.6	-	-
193654	32–33	32.5	*Sphagnum* stems/leaves	200 ± 15	-26.1	202	0–284
179329	44–45	44.4	*Sphagnum* stems/leaves	185 ± 20	-23.9	186	0–281
185567	56–57	56.4	125–250 µm bulk peat & *Sphagnum* stems/leaves	395 ± 15	-26.0	399	327–491
193655	60–61	60.6	*Sphagnum* stems/leaves	690 ± 15	-26.6	598	561–657
193656	65–66	66	*Sphagnum* stems/leaves	1130 ± 20	-26.4	981	934–1056
185568	70–71	71.2	*Sphagnum* stems/leaves	1270 ± 15	-24.7	1131	1069–1184
193657	76–77	77.3	*Sphagnum* stems/leaves	1610 ± 15	-26.9	1462	1411–1523
185569	82–83	83.6	*Sphagnum* stems/leaves	1740 ± 15	-26.7	1600	1543–1698
179331	90–91	91.7	*Sphagnum* stems/leaves	1905 ± 20§	-25.1	1793	1734–1870
193658	96–97	98.3	*Sphagnum* stems/leaves	1910 ± 15§	-26.5	1798	1742–1868
185570	108–109	109	*Sphagnum* stems/leaves	1915 ± 15§	-25.1	1810	1744–1872
179333	131–132	131.6	*Sphagnum* stems/leaves	3275 ± 20	-25.3	3450	3382–3557
179330	159–160	160	*Sphagnum* stems/leaves	3865 ± 20	-26.3	4212	4094–4400
179332	203–204	203.6	>63 µm bulk peat	4660 ± 20	-27.8	5410	5295–5462

* Some drives of peat core were slightly compressed during transport from field to lab, and for each subsample we used their corrected depths, assuming uniform compression of an individual core drive.

[#] Radiocarbon ages were calibrated to calendar ages using SHCal 13 dataset (Hogg et al., 2013) with Calib v7.10 (http://calib.org/calib/calib.html).

[†] These are post-bomb ^{14}C dates, which were originally reported as the fraction relative to modern ^{14}C (FM). Using calibration curve of Bomb 13 SH 1–2 dataset (Hua et al., 2013) on OxCal v4.3 (https://c14.arch.ox.ac.uk/oxcal/OxCal.html), sample 185565 was calibrated to A.D. 1959 (7.8% probability) and A.D. 1993 (87.6%). Sample 185566 was calibrated to A.D. 1963 (1.8%) and A.D. 1978 (93.6%). For the first sample, considering the stratigraphic position, we rejected the possibility of A.D. 1959 and assigned it an age of A.D. 1993. For the second sample, considering accumulation rates, we assigned its age at A.D. 1963 as that better fitted the expected peat accumulation pattern. In Bacon program (Blaauw and Christen, 2011), we input these two dates manually to their calibrated calendar years to avoid modeling age-depth relationships based simply on probability of post-bomb dates.

[§] Three identical ^{14}C dates within the uncertainty range suggested rapid accumulation of *Sphagnum* peat in this interval.

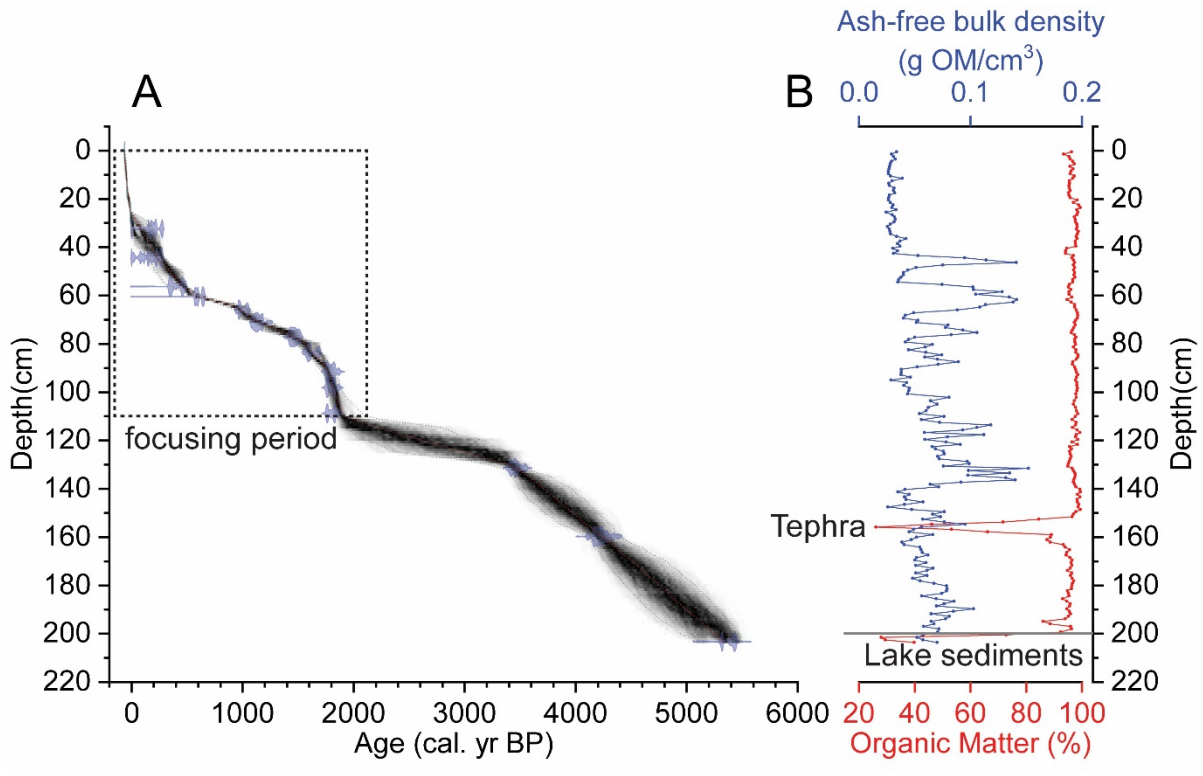

Figure DR2. (A) Bacon age-depth model of core PAT16-AP1 (Blaauw and Christen, 2011). (B) Organic matter percentage and ash-free bulk density of peat core from loss-on-ignition (LOI) analysis. The down-core variation of ash-free bulk density mainly reflected changes in botanical composition and the degree of decomposition of peat (Loisel et al., 2014). Organic matter percentage was higher than 95% throughout the core with very low mineral materials, except a tephra layer at 154–157 cm, suggesting the absence of fluvial influence on the peat bog.

3. Macrofossil analysis from Ariel Peatland

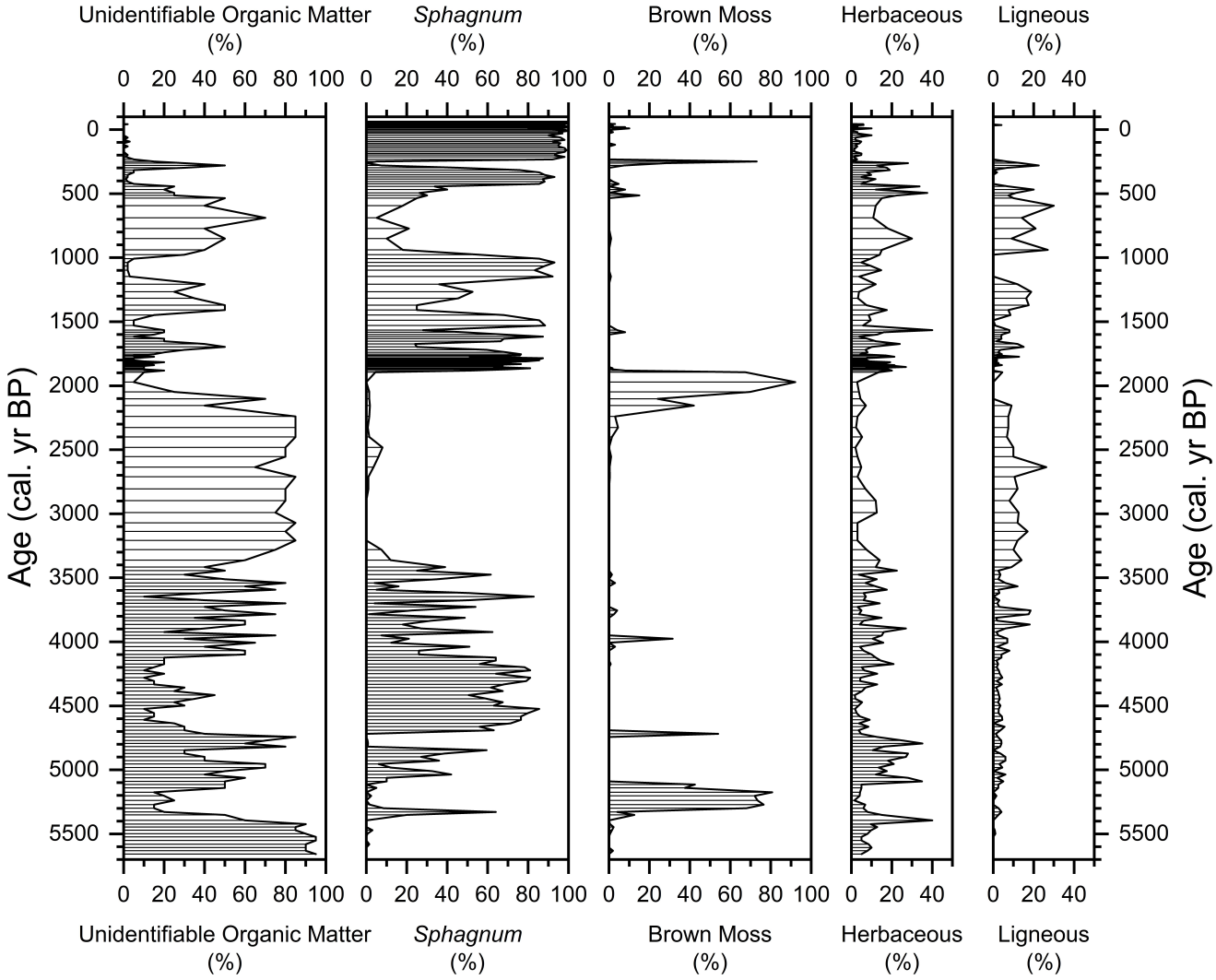

Figure DR3. Peat component and macrofossil diagram of peat core PAT16-AP1. The lowest section (older than 5400 cal. yr BP based on interpolated ages) was likely lake sediments with low organic matter (<30%; Fig. DR2). The apparent gap of *Sphagnum* from 3200 cal. yr BP to 1900 cal. yr BP led us to develop a *Sphagnum*-specific cellulose isotope record only for the past two millennia. *Sphagnum* macrofossils shown here are all from *S. magellanicum* as we did not find macrofossils of any other species (such as *S. cuspidatum*) in the core that could be present at wet locations near hollows and pools.

4. Evaluation of evaporative effect on oxygen isotopes of moss cellulose

We conducted a modern process study using surface *Sphagnum* samples across a hummock-hollow microtopographic gradient to further understand the influence of moisture condition on stable isotope compositions in *Sphagnum* cellulose. Site Valle de Consejo (VC; Fig. DR1C), located at about 4.5 km west to our peat-core study site AP, has considerable developments of surface hummock-hollow patterning, creating an ideal setting to carry out modern process study. In addition to field measurements of *in situ* hydrological variables, we collected *Sphagnum* samples at every 30-cm along a north-facing hummock-hollow transect of >400 cm in length and extracted cellulose from *Sphagnum* capitula (the very top of actively growing portion of mosses that represents the recent growth, i.e., during the summer) and then carried out isotope analysis following the same lab procedure as for down-core samples. Our results showed a strong negative correlation between $\delta^{18}O_{cell}$ and $\delta^{13}C_{cell}$ values ($r = -0.8$; $p < 0.001$), implying a common environmental factor governing the intra-site variation of both isotope ratios (Fig. DR5). Likewise, this negative correlation was also found from another similar study at a *Sphagnum*-dominated peatland site in southernmost Patagonia (Fig. DR5; Loader et al., 2016). Many studies on carbon isotope composition of mosses concluded that moisture availability exerts a critical influence (Rice and Giles, 1996; Price et al., 1997; Ménot and Burns, 2001; Loisel et al., 2009), although other studies indicated potential influence of temperature, probably due to intrinsic relation between temperature and moisture-related environmental factors (e.g., Ménot and Burns, 2001; Moschen et al., 2011). Other influencing factors include CO_2 concentration (White et al., 1994) and recycled CH_4-derived CO_2 (Price et al., 1997). On the other hand, oxygen isotope composition of mosses is mainly controlled by the oxygen isotope composition of meteoric water and its subsequent evaporative enrichment in ^{18}O of leaf water. For moss samples along our local hydrological transect, they should receive the same source of moisture, i.e., from precipitation. Therefore, evaporative enrichment played a key role modifying/elevating the source water $\delta^{18}O$ values (Ménot-Combes et al., 2002; Zanazzi and Mora, 2005). Our calibration data from site

VC showed that $\delta^{18}O_{cell}$ values had a range of ~18–21‰ (Fig. DR4). We made the following two assumptions to quantify the evaporative enrichment on $\delta^{18}O_{cell:}$

(1) Summer precipitation input has an average $\delta^{18}O$ value of about −10‰ based on the Global Network of Isotopes in Precipitation (GNIP) data in Ushuaia, the nearest GNIP station to our study site, also located on the east side of the Andes divide.

(2) Biochemical enrichment factor (ε_b) during cellulose biosynthesis has a constant value of ca. +27‰ that has been widely accepted in the literature (e.g., Zanazzi and Mora, 2005; Sternberg, 2009; Daley et al., 2010; Sternberg and Ellsworth, 2011). This fractionation factor seems to be conservative and independent of species (Daley et al., 2010). Recently, this biochemical enrichment factor has been considered to be temperature-dependent (Sternberg and Ellsworth, 2011):

$$\varepsilon_b = 0.0073T^2 - 0.4375T + 35.528$$

where T denotes temperature. If using average summer day-time temperature (~15 °C) in our study region (Loader et al., 2016), the temperature-calibrated ε_b would be slightly higher, at around +27.5 ‰. However, it should be noted that the ε_b-temperature relationship reported by Sternberg and Ellsworth (2011) was based on limited number of data and did not provide the uncertainty range. Thereafter, we still used +27‰ as the value of ε_b to estimate the extent of evaporative enrichment shown below.

We then calculated the hypothetical values of $\delta^{18}O_{cell}$ without considering any evaporative enrichment in leaf water using the equation (Daley et al., 2010):

$$\delta^{18}O_{cell} = \delta^{18}O_p + \varepsilon_b$$

The derived hypothetical $\delta^{18}O_{cell}$ value is ~17‰, which is at least about 1‰ lower than the $\delta^{18}O_{cell}$ values (~18–21‰) observed from the surface *Sphagnum* samples. We thus concluded that the extent of evaporative enrichment contributed an offset of ca. 1–4‰ between $\delta^{18}O_{cell}$ and $\delta^{18}O_p$. The uncertainties in $\delta^{18}O_p$ and ε_b values would only influence the magnitude of evaporative

enrichment, but they would not hamper our inference that evaporation isotopically enriched the leaf water, and played a key role modifying/elevating $\delta^{18}O_{cell}$ values.

We suggest that moisture condition or evaporative enrichment are the only possible mechanism to explain the negative correlation between $\delta^{18}O_{cell}$ and $\delta^{13}C_{cell}$ in our dataset. Hummock-growing *Sphagnum* mosses are away from the water table and thus drier with a thinner water film, which results in stronger discrimination against atmospheric $^{13}CO_2$ and lower $\delta^{13}C_{cell}$ values. Because hummock-growing *Sphagnum* are in deficiency of water, moss leaf water is subject to enhanced evaporative enrichment in ^{18}O, resulting in higher $\delta^{18}O_{cell}$ values. By contrast, hollow-growing *Sphagnum* mosses are near the water table and thus wetter with a thicker water film, which results in less discrimination against atmospheric $^{13}CO_2$ and higher $\delta^{13}C_{cell}$ values. Also, leaf water in hollow-growing *Sphagnum* mosses are near saturated, and leaf water is more protected from evaporative enrichment, which results in lower $\delta^{18}O_{cell}$ values. Therefore, we propose that paired measurements of moss $\delta^{18}O_{cell}$ and $\delta^{13}C_{cell}$ in the same cellulose samples allow us to elucidate the effect of moisture condition or evaporation in peat-core analysis (Xia et al., in prep.). If negative correlations between those isotopes were also found in peat cores, the relationships likely indicated changes in bog surface moisture conditions. However, in our peat-core analysis of core PAT16-AP1, we did not observe such negative correlation. Therefore, we conclude that moisture condition or evaporation are unlikely to be the dominant factors that explain the changes in $\delta^{18}O_{cell}$. Instead $\delta^{18}O_{cell}$ primarily document changes in $\delta^{18}O_p$.

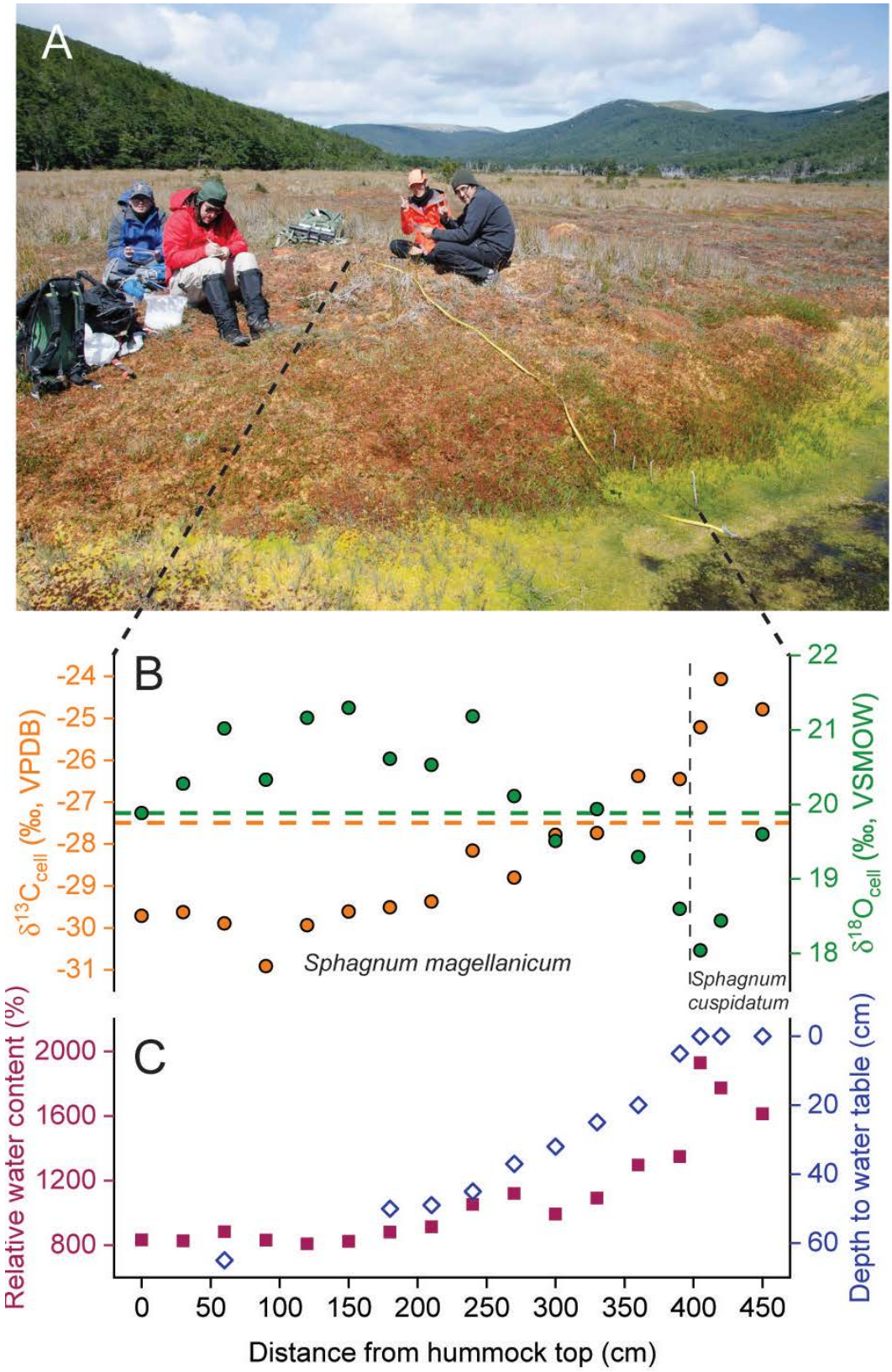

Figure DR4. (A) Field photo of the hummock-hollow transect at site Valle de Consejo (VC) for our modern process study. (B) *Sphagnum* $\delta^{18}O_{cell}$ (green circles) and $\delta^{13}C_{cell}$ (orange circles) variations across hummock-hollow

hydrological gradient. Data points on the right side of black vertical dashed line are from different species: green-color *S. cuspidatum*. Green and orange horizontal dashed lines are the $\delta^{18}O_{cell}$ and $\delta^{13}C_{cell}$ values of surface *Sphagnum* moss capitula from the coring location of site Ariel Peatland. (C) Field measurements of relative water content (water mass/dry moss mass; pink filled squares) and water table depth (blue open diamonds) on the hummock-hollow transect.

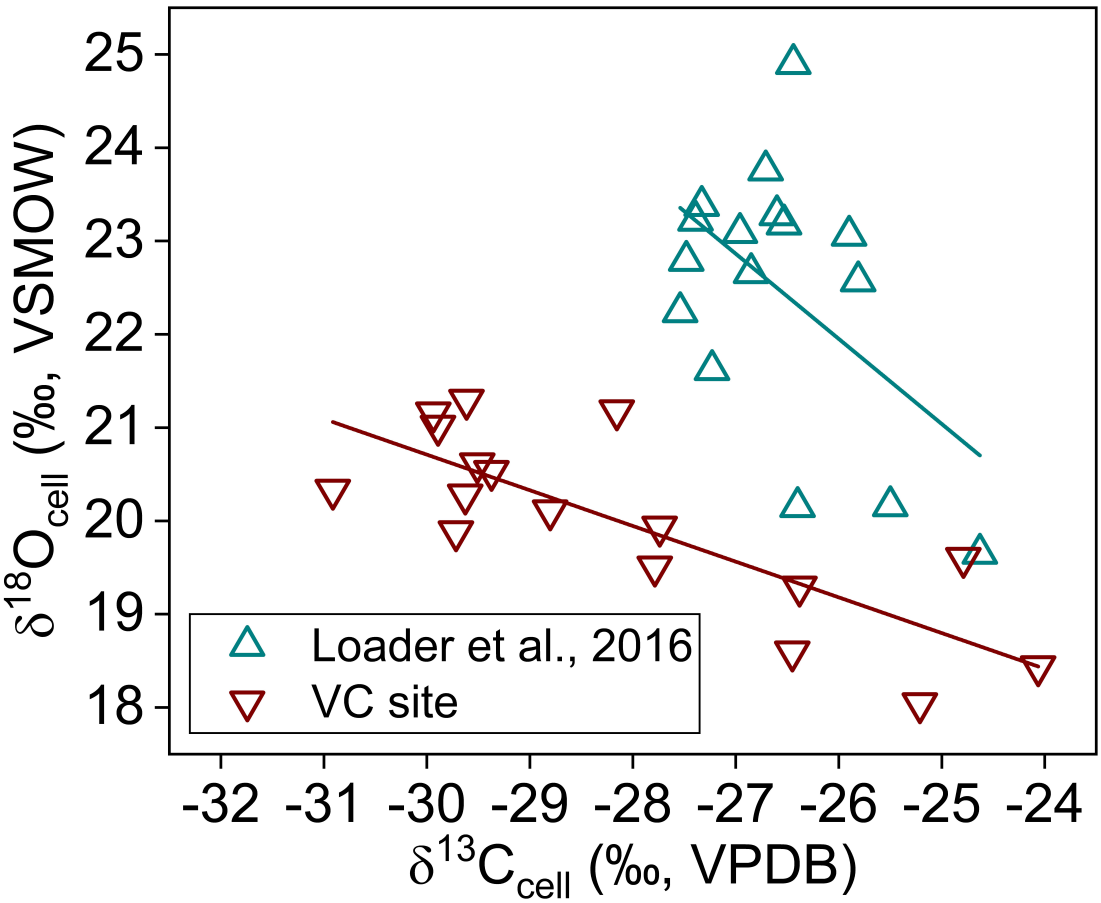

Figure DR5. Negative correlation between *Sphagnum* $\delta^{18}O_{cell}$ and $\delta^{13}C_{cell}$ from surface samples along hydrological gradient within a single site. Data from site VC (Fig. DR4) show negative correlation ($r = -0.8$, $p < 0.001$) with a slope of −0.38 in regression line. Data from the site in Laguna Parrillar National Reserve about 35 km southwest to Punta Arenas were collected across multiple hummock-hollow transects (Loader et al., 2016) but a weaker negative correlation ($r = -0.51$, $p < 0.05$) with a slope of −0.91 in regression line could still be found.

5. Air-parcel backward trajectory analysis using HYSPLIT model

We used a Python package (PySPLIT; Cross, 2015) interfaced with NOAA's HYbrid Single-Particle Lagrangian Integrated Trajectory (HYSPLIT) (Stein et al., 2015) to analyze the backward trajectories of rainfall-producing air masses from our study site Ariel Peatland. We used the Global Data Assimilation System (GDAS) at 1° × 1° resolution as the gridded meteorological data. By running the "mass-production" trajectory generation code in PySPLIT, we calculated 120-hour back-trajectories at every 6-hour interval for September–May (austral spring, summer and autumn, i.e., most likely growing seasons) during the period 2005–2017. Air parcels were initialized at 500 m, 1000 m, 1500 m, and 2000 m above ground level (AGL), but we restricted following analysis to only trajectories with initialization altitude at 500-m AGL (~900 mb) as air parcel movements at this level are more sensitive to synoptic conditions, particularly to the days with easterly winds (Agosta et al., 2015). We further filtered trajectories based on two criteria: (1) trajectory is rainfall-producing at starting point (time = 0); and (2) integration error calculated from "reverse trajectory" is lower than two units of standard deviation of the mean (Cross, 2015; Scroxton et al., 2017). This resulted in total of 2506 trajectories, which were then binned by 1° × 1° to count the trajectory frequency and produce frequency contour (Caves et al., 2015). We then used Python to further extract the back-trajectories that passed over the Atlantic Ocean within 20 hours before arriving the location (Fig. DR6). Monthly percentage of easterly-related trajectories during the months from September to May in the period 2005–2017, were then used to investigate the correlation with European Centre for Medium-Range Weather Forecasts (ECMWF) ERA-Interim sea level pressure on Climate Explorer (http://climexp.knmi.nl) (Krklec and Domínguez-Villar, 2014).

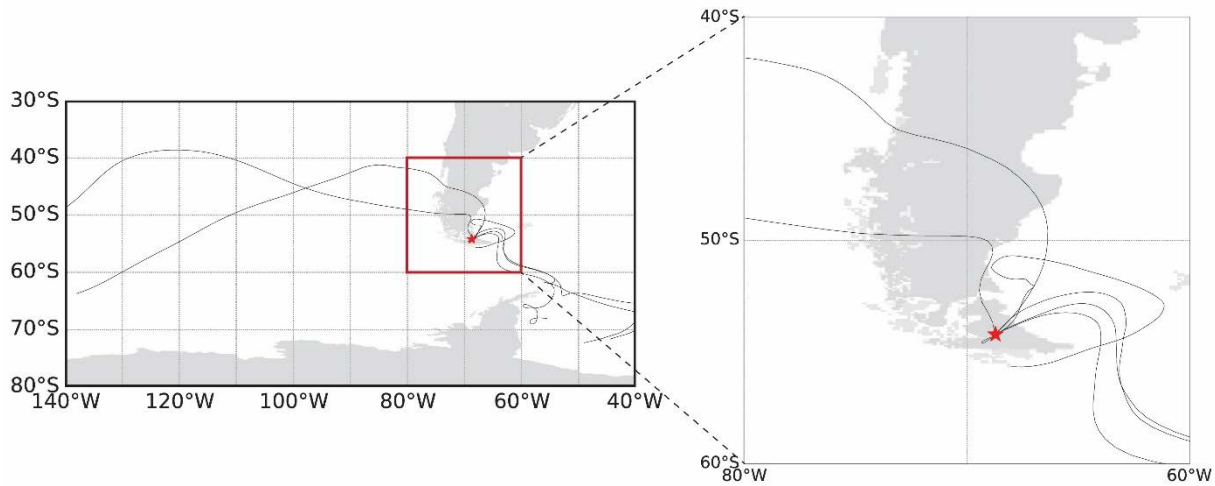

Figure DR6. Easterly-related trajectories extracted from rainfall-producing trajectories in April 2017 as an example. Red star is our study site Ariel Peatland.

6. A close-up look of PAT16-AP1 proxy record for the last 150 years

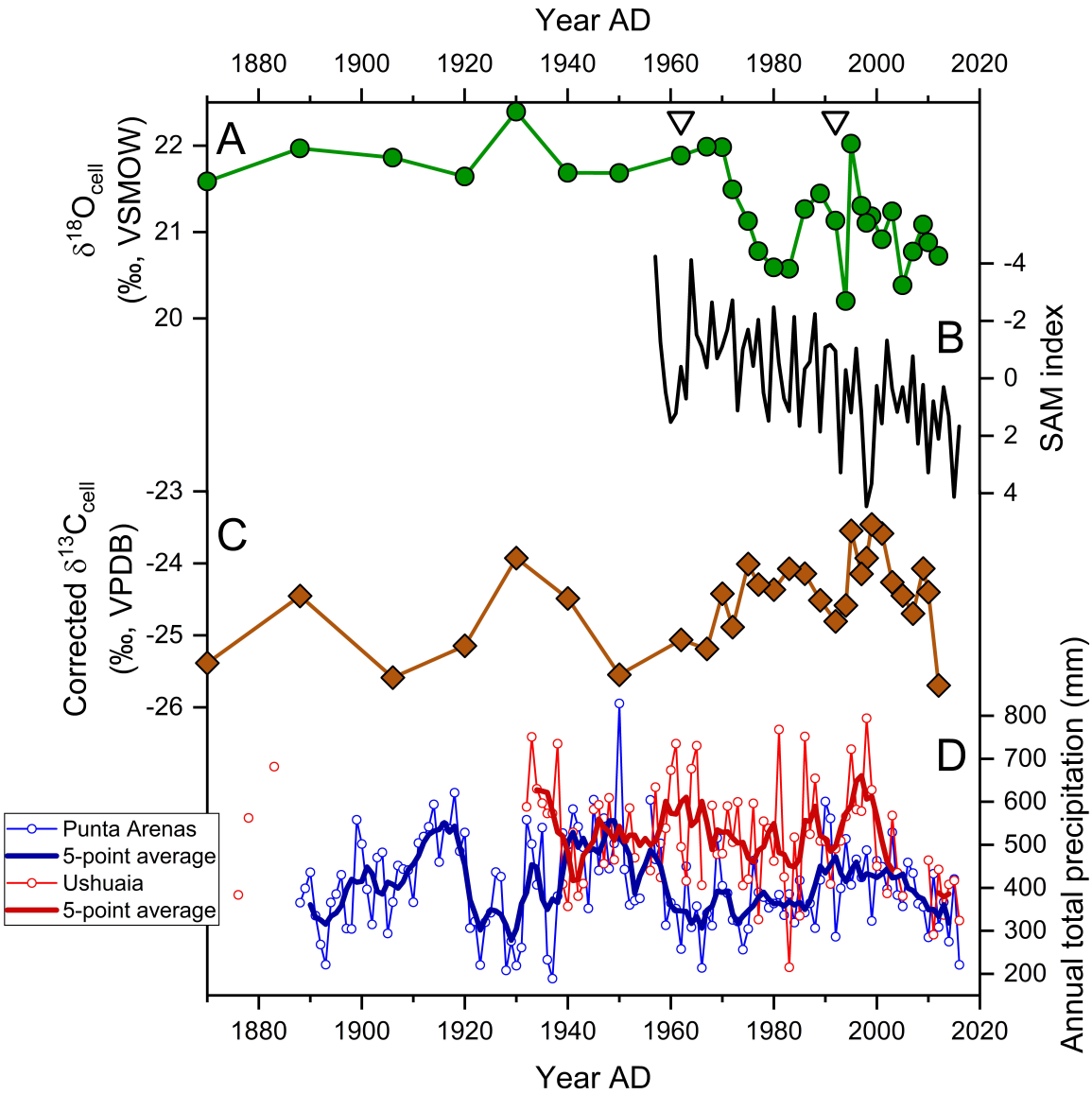

Figure DR7. A close-up look at proxy records of peat core PAT16-AP1 during the recent 150 years in comparison with instrumental records. (A) *Sphagnum* $\delta^{18}O_{cell}$ record. (B) Marshall annual SAM index (reverse scale on *y*-axis). (C) *Sphagnum* corrected $\delta^{13}C_{cell}$ record. (D) Punta Arenas and Ushuaia station-based annual total precipitation records; data source is the Global Historical Climatology Network (GHCN) dataset. Triangles on top are the level dated by post-bomb radiocarbon (Table DR1).

References Cited

Agosta, E., Compagnucci, R., and Ariztegui, D., 2015, Precipitation linked to Atlantic moisture transport: clues to interpret Patagonian palaeoclimate: Climate Research, v. 62, p. 219–240, https://doi.org/10.3354/cr01272.

Blaauw, M. and Christen, J.A., 2011, Flexible paleoclimate age-depth models using an autoregressive gamma process: Bayesian analysis, v. 6, p. 457–474, https://doi.org/10.1214/ba/1339616472.

Caves, J.K., Winnick, M.J., Graham, S.A., Sjostrom, D.J., Mulch, A., and Chamberlain, C.P., 2015, Role of the westerlies in Central Asia climate over the Cenozoic: Earth and Planetary Science Letters, v. 428, p. 33–43, https://doi.org/10.1016/j.epsl.2015.07.023.

Cross, M., 2015, PySPLIT: a package for the generation, analysis, and visualization of HYSPLIT air parcel trajectories, Proc. of the 14th Python in Science Conf., p. 137–142.

Daley, T.J., Barber, K.E., Street-Perrott, F.A., Loader, N.J., Marshall, J.D., Crowley, S.F., and Fisher, E.H., 2010, Holocene climate variability revealed by oxygen isotope analysis of *Sphagnum* cellulose from Walton Moss, northern England: Quaternary Science Reviews, v. 29, p. 1590–1601, https://doi.org/10.1016/j.quascirev.2009.09.017.

Hogg, A.G., et al., SHCal13 Southern Hemisphere Calibration, 0–50,000 Years cal BP: Radiocarbon, v. 55, 1889–1903, https://doi.org/10.2458/azu_js_rc.55.16783.

Hua, Q., Barbetti, M., and Rakowski, A.Z., 2013, Atmospheric Radiocarbon for the Period 1950–2010: Radiocarbon, v. 55, p. 2059–2072, https://doi.org/10.2458/azu_js_rc.v55i2.16177.

Krklec, K., and Domínguez-Villar, D., 2014, Quantification of the impact of moisture source regions on the oxygen isotope composition of precipitation over Eagle Cave, central Spain: Geochimica et Cosmochimica Acta, v. 134, p. 39–54, https://doi.org/10.1016/j.gca.2014.03.011.

Loader, N.J., et al., 2016, Measurements of hydrogen, oxygen and carbon isotope variability in *Sphagnum* moss along a micro-topographical gradient in a southern Patagonian peatland: Journal of Quaternary Science, v. 31, p. 426–435, https://doi.org/10.1002/jqs.2871.

Loisel, J., Garneau, M., and Hélie, J.-F., 2009, Modern *Sphagnum* $\delta^{13}C$ signatures follow a surface moisture gradient in two boreal peat bogs, James Bay lowlands, Québec: Journal of Quaternary Science, v. 24, p. 209–214, https://doi.org/10.1002/jqs.1221.

Loisel, J., and Yu, Z., 2013, Holocene peatland carbon dynamics in Patagonia: Quaternary Science Reviews, v. 69, p. 125–141, https://doi.org/10.1016/j.quascirev.2013.02.023.

Loisel, J., et al., 2014, A database and synthesis of northern peatland soil properties and Holocene carbon and nitrogen accumulation: The Holocene, v. 24, p. 1028–1042, https://doi.org/10.1177/0959683614538073.

Ménot-Combes, G., Burns, S.J., and Leuenberger, M., 2002, Variations of $^{18}O/^{16}O$ in plants from temperate peat bogs (Switzerland): implications for paleoclimatic studies: Earth and Planetary Science Letters, v. 202, p. 419–434, https://doi.org/10.1016/S0012-821X(02)00794-X.

Ménot, G., and Burns, S.J., 2001, Carbon isotopes in ombrogenic peat bog plants as climatic indicators: calibration from an altitudinal transect in Switzerland: Organic Geochemistry, v. 32, p. 233–245, https://doi.org/10.1016/S0146-6380(00)00170-4.

Moschen, R., Kühl, N., Peters, S., Vos, H., and Lücke, A., 2011, Temperature variability at Dürres Maar, Germany during the Migration Period and at High Medieval Times, inferred from stable carbon isotopes of *Sphagnum* cellulose: Clim. Past, v. 7, p. 1011–1026, https://doi.org/10.5194/cp-7-1011-2011.

Price, G.D., McKenzie, J.E., Pilcher, J.R., and Hoper, S.T., 1997, Carbon-isotope variation in *Sphagnum* from hummock-hollow complexes: implications for Holocene climate reconstruction: The Holocene, v. 7, p. 229–233, https://doi.org/10.1177/095968369700700211.

Rice, S.K., and Giles, L., 1996, The influence of water content and leaf anatomy on carbon isotope discrimination and photosynthesis in *Sphagnum*: Plant, Cell & Environment, v. 19, p. 118–124, https://doi.org/10.1111/j.1365-3040.1996.tb00233.x.

Scroxton, N., Burns, S.J., McGee, D., Hardt, B., Godfrey, L.R., Ranivoharimanana, L., and Faina, P., 2017, Hemispherically in-phase precipitation variability over the last 1700 years in a Madagascar speleothem record: Quaternary Science Reviews, v. 164, p. 25–36, https://doi.org/10.1016/j.quascirev.2017.03.017.

Stein, A.F., Draxler, R.R., Rolph, G.D., Stunder, B.J.B., Cohen, M.D., and Ngan, F., 2015, NOAA's HYSPLIT Atmospheric Transport and Dispersion Modeling System:

Bulletin of the American Meteorological Society, v. 96, p. 2059–2077, https://doi.org/10.1175/bams-d-14-00110.1.

Sternberg, L., and Ellsworth, P.F.V., 2011, Divergent Biochemical Fractionation, Not Convergent Temperature, Explains Cellulose Oxygen Isotope Enrichment across Latitudes: PLOS ONE, v. 6, e28040, https://doi.org/10.1371/journal.pone.0028040.

Sternberg, L.d.S.L.O.R., 2009, Oxygen stable isotope ratios of tree-ring cellulose: the next phase of understanding: New Phytologist, v. 181, p. 553–562, https://10.1111/j.1469-8137.2008.02661.x.

White, J.W.C., Ciais, P., Figge, R.A., Kenny, R., and Markgraf, V., 1994, A high-resolution record of atmospheric CO_2 content from carbon isotopes in peat: Nature, v. 367, 153–156, https://10.1038/367153a0.

Zanazzi, A., and Mora, G., 2005, Paleoclimatic implications of the relationship between oxygen isotope ratios of moss cellulose and source water in wetlands of Lake Superior: Chemical Geology, v. 222, p. 281–291, https://doi.org/10.1016/j.chemgeo.2005.08.006.